Coupled Tensor Decompositions in Array Processing

Mikael Sørensen and Lieven De Lathauwer, *Senior Member, IEEE*

***Abstract*—The Canonical Polyadic Decomposition (CPD) plays an important role in array processing in the case of arrays composed of several displaced but identical subarrays. However, the CPD model is less appropriate for more complex array geometries. As our first contribution, we present a paradigm shift from the conventional matrix/tensor decomposition approach to coupled matrix/tensor based array processing. More precisely, we propose the coupled CPD model as a new algebraic framework for array processing. In particular, we demonstrate that the coupled CPD can handle array processing problems involving multiple shift-invariance structures. This leads to new uniqueness conditions and algebraic multidimensional ESPRIT methods for many antenna array configurations found in the literature. Second, we also present a link between wideband vector-sensor array processing and the coupled CPD. This leads to a new coherent data processing framework for VSA that takes the wideband structure of the signals into account.**

***Index Terms*—array processing, direction-of-arrival, source separation, tensors, coupled decompositions.**

I. Introduction

Sensor arrays have found important applications in radar, sonar, wireless communication and medical diagnostics. The connection between sensor array processing problems with regular geometries and tensors was recognized in [24]. More precisely, a link between the CPD and arrays composed of several displaced but identical subarrays [22], [35], [34], [36], [15] was presented in [24].

In practice, the array geometries may be irregular, the subarrays may be sparse, different or some of the sensors (or equivalently some sensor outputs) may be missing. As already pointed out in [24] a notable limitation of the CPD is that it can only handle (very) regular array geometries. Even for very regular geometries, such as the Uniform Rectangular Array (URA), very few algebraic studies are known to the authors. Hence, the need for a flexible and algebraic framework for array processing that can improve and break the confinements of the standard CPD approach is apparent.

To overcome some of the limitations of traditional array signal processing, the authors suggest a shift from the conventional matrix/tensor decomposition approach to coupled matrix/tensor based array processing. In this paper we argue that the coupled CPD framework presented in [29], [32] is a good framework for array processing. Part of this work was presented in the conference paper [26].

We first demonstrate that the coupled CPD provides a unified algebraic framework for one-, two-, three- or N-dimensional arrays with shift-invariance structures. In particular, the coupled CPD framework yields new dedicated uniqueness conditions and algorithms for many array geometries proposed in the literature, such as rectangular shaped, hexagonal shaped, cross-shaped, frame-shaped, L-shaped, V-shaped, Y-shaped, triangular shaped, octagon shaped and multi-scale invariance arrays (e.g. [12], [11], [39], [37], [7], [14], [37], [9], [8], [17]).

Second, we briefly explain that the coupled CPD appears in Vector-Sensor Array (VSA) processing [19], [18]. In particular, the coupled CPD provides a coherent data processing framework for VSA in the case of wideband signals which is relevant in the context of acoustic (e.g. [1], [16], [38]) or seismic signal processing (e.g. [6], [20]).

Even though we only focus on applications in array processing, multiple shift-invariance structured problems appear in a wide range of areas such as multi-sensor data fusion, multi-modal biomedical engineering and multi-set data mining. See [29], [32], [25] for references to concrete applications. As such, the concepts presented in this paper are relevant beyond array processing.

The paper is organized as follows. The rest of the introduction will present the notation. Section II reviews the necessary algebraic prerequisites. Section III discusses unconstrained and constrained CPD based array processing. Section IV introduces the coupled CPD framework for array processing problems involving array geometries with multiple shift-invariance structures. Section V briefly explains that the coupled CPD also provides a framework for VSA processing, even in the case of random array geometries. Numerical experiments are reported in section VI. Section VII concludes the paper.

A. Notation

Vectors, matrices and tensors are denoted by lower case boldface, upper case boldface and upper case calligraphic letters, respectively. The rth column, conjugate, transpose, conjugate-transpose, range, kernel, real and imaginary part of a matrix $\mathbf{A}$ are denoted by $\mathbf{a}_r$, $\mathbf{A}^*$, $\mathbf{A}^T$, $\mathbf{A}^H$, $\text{range}(\mathbf{A})$, $\ker(\mathbf{A})$, $\text{Re}\{\mathbf{A}\}$ and $\text{Im}\{\mathbf{A}\}$, respectively.

M. Sørensen and L. De Lathauwer are with KU Leuven - E.E. Dept. (ESAT) - STADIUS Center for Dynamical Systems, Signal Processing and Data Analytics, Kasteelpark Arenberg 10, B-3001 Leuven-Heverlee, Belgium, the Group Science, Engineering and Technology, KU Leuven Kulak, E. Sabbelaan 53, 8500 Kortrijk, Belgium, and iMinds Medical IT, Kasteelpark Arenberg 10, B-3001 Leuven-Heverlee, Belgium, {Mikael.Sorensen, Lieven.DeLathauwer}@kuleuven-kulak.be.

The symbols $\otimes$ and $\odot$ denote the Kronecker and Khatri-Rao product, defined as

$$\mathbf{A}\otimes\mathbf{B} \triangleq \begin{bmatrix} a_{11}\mathbf{B} & a_{12}\mathbf{B} & \dots \\ a_{21}\mathbf{B} & a_{22}\mathbf{B} & \dots \\ \vdots & \vdots & \ddots \end{bmatrix}, \quad \mathbf{A}\odot\mathbf{B} \triangleq [\mathbf{a}_1\otimes\mathbf{b}_1 \;\; \mathbf{a}_2\otimes\mathbf{b}_2 \;\; \dots],$$

in which $(\mathbf{A})_{mn} = a_{mn}$. The outer product of, say three vectors $\mathbf{a}$, $\mathbf{b}$ and $\mathbf{c}$ is denoted by $\mathbf{a}\circ\mathbf{b}\circ\mathbf{c}$, such that $(\mathbf{a}\circ\mathbf{b}\circ\mathbf{c})_{ijk} = a_i b_j c_k$. From the context it should be clear when i denotes the imaginary unit number, i.e., $i = \sqrt{-1}$.

The exchange matrix with unit entries on the counter-diagonal and zeros elsewhere is denoted by $\mathbf{J}_I \in \mathbb{C}^{I\times I}$.

$D_k(\mathbf{A}) \in \mathbb{C}^{J\times J}$ denotes the diagonal matrix holding row k of $\mathbf{A} \in \mathbb{C}^{I\times J}$ on its diagonal. Matlab index notation will be used for submatrices of a given matrix. For example, $\mathbf{A}(1{:}k,:)$ represents the submatrix of $\mathbf{A}$ consisting of the rows from 1 to k of $\mathbf{A}$. Let $\mathbf{A} \in \mathbb{C}^{I\times R}$, then $\underline{\mathbf{A}} = \mathbf{A}(1:I-1,:) \in \mathbb{C}^{(I-1)\times R}$, i.e., $\underline{\mathbf{A}}$ is obtained by deleting the bottom row of $\mathbf{A}$.

The binomial coefficient is denoted by $C_m^k = \frac{m!}{k!(m-k)!}$. The k-th compound matrix of $\mathbf{A} \in \mathbb{C}^{I\times R}$ is denoted by $C_k(\mathbf{A}) \in \mathbb{C}^{C_I^k \times C_R^k}$. It is the matrix containing the determinants of all $k\times k$ submatrices of $\mathbf{A}$, arranged with the submatrix index sets in lexicographic order, see [3] and references therein for a discussion.

II. Algebraic Prerequisites

A. Canonical Polyadic Decomposition (CPD)

Consider the third-order tensor $\mathcal{X} \in \mathbb{C}^{I\times J\times K}$. We say that $\mathcal{X}$ is a rank-1 tensor if it is equal to the outer product of some non-zero vectors $\mathbf{a} \in \mathbb{C}^I$, $\mathbf{b} \in \mathbb{C}^J$ and $\mathbf{c} \in \mathbb{C}^K$ such that $x_{ijk} = a_i b_j c_k$. A Polyadic Decomposition (PD) is a decomposition of $\mathcal{X}$ into a sum of rank-1 terms:

$$\mathbb{C}^{I\times J\times K} \ni \mathcal{X} = \sum_{r=1}^{R} \mathbf{a}_r \circ \mathbf{b}_r \circ \mathbf{c}_r \,. \tag{1}$$

The rank of a tensor $\mathcal{X}$ is equal to the minimal number of rank-1 tensors that yield $\mathcal{X}$ in a linear combination. Assume that the rank of $\mathcal{X}$ is R, then (1) is called the CPD of $\mathcal{X}$. Let us stack the vectors $\{\mathbf{a}_r\}$, $\{\mathbf{b}_r\}$ and $\{\mathbf{c}_r\}$ into the matrices $\mathbf{A} = [\mathbf{a}_1,\dots,\mathbf{a}_R]$, $\mathbf{B} = [\mathbf{b}_1,\dots,\mathbf{b}_R]$ and $\mathbf{C} = [\mathbf{c}_1,\dots,\mathbf{c}_R]$. The matrices $\mathbf{A}$, $\mathbf{B}$ and $\mathbf{C}$ will be referred to as the factor matrices of the PD or CPD of $\mathcal{X}$.

1) Matrix Representation: Let $\mathbf{X}^{(i\cdot\cdot)} \in \mathbb{C}^{J\times K}$ denote the matrix such that $\left(\mathbf{X}^{(i\cdot\cdot)}\right)_{jk} = x_{ijk}$, then $\mathbf{X}^{(i\cdot\cdot)} = \mathbf{B}D_i(\mathbf{A})\mathbf{C}^T$ and we obtain the following matrix representation of (1):

$$\mathbb{C}^{IJ\times K} \ni \mathbf{X}_{(1)} := \left[\mathbf{X}^{(1\cdot\cdot)T},\dots,\mathbf{X}^{(I\cdot\cdot)T}\right]^T = (\mathbf{A}\odot\mathbf{B})\mathbf{C}^T. \tag{2}$$

2) Uniqueness: The uniqueness properties of the CPD have been intensely studied in recent years, see [3], [4], [31] and references therein. In this paper we consider the case where at least one factor has full column rank. In wireless communication and radar processing this typically corresponds to the factor matrix in which transmitted symbols or data snapshots are stacked, respectively. For this case the following sufficient uniqueness condition has been obtained.

Theorem II.1. *Consider the PD of $\mathcal{X} \in \mathbb{C}^{I\times J\times K}$ in (1). If*

$$\begin{cases} \boldsymbol{C} \text{ has full column rank,} \\ C_2(\boldsymbol{A}) \odot C_2(\boldsymbol{B}) \text{ has full column rank,} \end{cases} \tag{3}$$

then the rank of $\mathcal{X}$ is R and the CPD of $\mathcal{X}$ is unique [13], [2], [3]. Generically[1], condition (3) is satisfied if $2R(R-1) \le I(I-1)J(J-1)$ and $R \le K$ [2].

The uniqueness condition (3) is relatively easy to check and yet very powerful. Moreover, under condition (3) the CPD can be computed by algebraic means [2]. More precisely, the CPD problem was reduced to a Simultaneous matrix Diagonalization (SD) problem. In the case of an exact CPD, the SD problem can be solved via a standard Generalized EigenValue Decomposition (GEVD). The approach has been further generalized to cases where $\mathbf{C}$ does not have full column rank [5]. For these reasons all CPD based uniqueness conditions stated in this paper will be derived from condition (3).

B. Vandermonde matrices

The matrix $\mathbf{A} \in \mathbb{C}^{I\times R}$ is called Vandermonde if

$$\mathbf{A} = [\mathbf{a}_1,\dots,\mathbf{a}_R], \quad \mathbf{a}_r = \left[1, z_r, z_r^2, \dots, z_r^{I-1}\right]^T, \tag{4}$$

where the scalars $\{z_r\}$ are called the generators of $\mathbf{A}$.

1) Forward-Backward Averaging (FBA): If the generators of the Vandermonde matrix $\mathbf{A}$ are located on the unit circle ($|z_r| = 1$), then we can make use of the well-known FBA procedure (e.g. [21]). More precisely, if $z_r = e^{i\alpha_r}$ where $\alpha_r \in \mathbb{R}$, $\forall r \in \{1,\dots,R\}$, then $\mathbf{J}_I\mathbf{A}^* = \mathbf{A}\mathbf{D}_\mathbf{A}$ in which $\mathbf{D}_\mathbf{A} = D_1\left(\left[z_1^{-(I-1)}, z_2^{-(I-1)}, \dots, z_R^{-(I-1)}\right]\right)$. FBA basically doubles the amount of observed data. As an example, consider the factorization $\mathbf{X} = \mathbf{A}\mathbf{S}^T$ in which $\mathbf{A}$ is Vandermonde with modulus norm generators. FBA now provides the augmented factorization $[\mathbf{X}, \mathbf{J}_I\mathbf{X}^*] = \mathbf{A}[\mathbf{S}^T, \mathbf{D}_\mathbf{A}\mathbf{S}^H]$.

2) Spatial smoothing: When working with Vandermonde matrices it is common to do spatial smoothing in a preprocessing step (e.g. [23]). Spatial smoothing can be used to increase the diversity of a system or to prevent ill-conditioned factor matrices. As an example (which will be used throughout the paper), consider the factorization $\mathbf{X} = \mathbf{A}\mathbf{S}^T \in \mathbb{C}^{I\times K}$ in which $\mathbf{A} \in \mathbb{C}^{I\times R}$ is of the form (4). Using $z_r^{l_1+k_1-2} = z_r^{l_1-1}z_r^{k_1-1}$, spatial smoothing maps $\mathbf{X}$ to $\mathbf{Y} = (\mathbf{A}^{(K_1)} \odot \mathbf{A}^{(L_1)})\mathbf{S}^T$ as follows

$$y_{(k_1-1)L_1+l_1,k} = x_{k_1+l_1-1,k}, \quad 1 \le k \le K_1\,,\; 1 \le l \le L_1\,,$$

[1] A tensor decomposition property is called generic if it holds with probability one when the entries of the factor matrices are drawn from absolutely continuous probability density measures.

subject to $K_1 + L_1 = I + 1$, in which $\mathbf{A}^{(K_1)} \in \mathbb{C}^{K_1 \times R}$ and $\mathbf{A}^{(L_1)} \in \mathbb{C}^{L_1 \times R}$ are given by

$$\mathbf{A}^{(L_1)} = \left[\mathbf{a}_1^{(L_1)}, \ldots, \mathbf{a}_R^{(L_1)}\right],\ \mathbf{a}_r^{(L_1)} = \left[1, z_r, z_r^2, \ldots, z_r^{L_1-1}\right]^T, \quad (5)$$

$$\mathbf{A}^{(K_1)} = \left[\mathbf{a}_1^{(K_1)}, \ldots, \mathbf{a}_R^{(K_1)}\right],\ \mathbf{a}_r^{(K_1)} = \left[1, z_r, z_r^2, \ldots, z_r^{K_1-1}\right]^T. \quad (6)$$

We can interpret $\mathbf{Y}$ as matrix representation of a CPD of a third-order tensor $\mathcal{Y} \in \mathbb{C}^{L_1 \times K_1 \times R}$. In other words, by going from a Vandermonde constrained matrix factorization of $\mathbf{X}$ to a Vandermonde constrained CPD with matrix representation $\mathbf{Y}$, the order of the data array has increased by one.

C. CPD with a Vandermonde factor matrix

Consider the PD of $\mathcal{X} \in \mathbb{C}^{I \times J \times K}$ in (1) where $\mathbf{A}$ is Vandermonde. Spatial smoothing yields $\mathbf{Y} \in \mathbb{C}^{K_1 J \times L_1 K}$ with

$$y_{(k_1-1)J+j,(l_1-1)K+k} = x_{l_1+k_1-1,j,k} = \sum_{r=1}^{R} z_r^{l_1-1} b_{j,r} z_r^{k_1-1} c_{k,r},$$

and matrix factorization

$$\mathbb{C}^{K_1 J \times L_1 K} \ni \mathbf{Y} = \left(\mathbf{A}^{(K_1)} \odot \mathbf{B}\right)\left(\mathbf{A}^{(L_1)} \odot \mathbf{C}\right)^T, \quad (7)$$

where $\mathbf{A}^{(L_1)} \in \mathbb{C}^{L_1 \times R}$ and $\mathbf{A}^{(K_1)} \in \mathbb{C}^{K_1 \times R}$ are given by (5) and (6) subject to $K_1 + L_1 = I + 1$. The following uniqueness condition was obtained in [28]. Note that in a Vandermonde constrained (C)PD the scaling/counterscaling indeterminacies do not involve the Vandermonde factors.

Theorem II.2. *Let $\mathcal{X} \in \mathbb{C}^{I \times J \times K}$ be given by* (1)*. Assume that $\boldsymbol{A}$ is a Vandermonde matrix with distinct generators. Consider the matrix representation* (7)*. If there exists a pair (K_1, L_1) subject to $K_1 + L_1 = I + 1$ such that*

$$\begin{cases} \underline{\boldsymbol{A}}^{(K_1)} \odot \boldsymbol{B} \text{ has full column rank,} \\ \boldsymbol{A}^{(L_1)} \odot \boldsymbol{C} \text{ has full column rank,} \end{cases} \quad (8)$$

then the Vandermonde constrained rank of $\mathcal{X}$ is R and the Vandermonde constrained CPD of $\mathcal{X}$ is unique. Generically, condition (8) *is satisfied if and only if $\left\lceil \frac{R}{J} \right\rceil + \left\lceil \frac{R}{K} \right\rceil \leq I$.*

The Vandermonde constrained CPD is unique under milder conditions than its unconstrained CPD counterpart. (Compare for instance Theorem II.1 with Theorem II.2). A GEVD-based algorithm for computing the CPD with a Vandermonde factor matrix was also provided in [28].

D. Coupled CPD

We say that a collection of tensors $\mathcal{X}^{(n)} \in \mathbb{C}^{I_n \times J_n \times K}$, $n \in \{1, \ldots, N\}$, admits an R-term coupled PD if each tensor $\mathcal{X}^{(n)}$ can be written as [28]:

$$\mathcal{X}^{(n)} = \sum_{r=1}^{R} \mathbf{a}_r^{(n)} \circ \mathbf{b}_r^{(n)} \circ \mathbf{c}_r, \quad n \in \{1, \ldots, N\}, \quad (9)$$

with factor matrices $\mathbf{A}^{(n)} = \left[\mathbf{a}_1^{(n)}, \ldots, \mathbf{a}_R^{(n)}\right]$, $\mathbf{B}^{(n)} = \left[\mathbf{b}_1^{(n)}, \ldots, \mathbf{b}_R^{(n)}\right]$ and $\mathbf{C} = [\mathbf{c}_1, \ldots, \mathbf{c}_R]$. We define the coupled rank of $\{\mathcal{X}^{(n)}\}$ as the minimal number of coupled rank-1 tensors $\mathbf{a}_r^{(n)} \circ \mathbf{b}_r^{(n)} \circ \mathbf{c}_r$ that yield $\{\mathcal{X}^{(n)}\}$ in a linear combination. Assume that the coupled rank of $\{\mathcal{X}^{(n)}\}$ is R, then (9) will be called the coupled CPD of $\{\mathcal{X}^{(n)}\}$.

The coupled PD or CPD of $\{\mathcal{X}^{(n)}\}$ has the following matrix representation

$$\mathbf{X} = \left[\mathbf{X}_{(1)}^{(1)T}, \ldots, \mathbf{X}_{(1)}^{(N)T}\right]^T = \mathbf{F}\mathbf{C}^T \in \mathbb{C}^{(\sum_{n=1}^{N} I_n J_n) \times K}, \quad (10)$$

where $\mathbf{F} = [(\mathbf{A}^{(1)} \odot \mathbf{B}^{(1)})^T, \ldots, (\mathbf{A}^{(N)} \odot \mathbf{B}^{(N)})^T]^T \in \mathbb{C}^{(\sum_{n=1}^{N} I_n J_n) \times R}$.

The coupled rank-1 tensors in (9) can be arbitrarily permuted and the vectors within the same coupled rank-1 tensor can be arbitrarily scaled provided the overall coupled rank-1 term remains the same. We say that the coupled CPD is unique when it is only subject to these trivial indeterminacies. Uniqueness conditions for the coupled CPD have been developed in [29]. Theorem II.3 extends Theorem II.1 to coupled CPD.

Theorem II.3. *Consider the coupled PD of $\mathcal{X}^{(n)} \in \mathbb{C}^{I_n \times J_n \times K}$, $n \in \{1, \ldots, N\}$ in* (9)*. Define*

$$\boldsymbol{G} = \begin{bmatrix} C_2\left(\boldsymbol{A}^{(1)}\right) \odot C_2\left(\boldsymbol{B}^{(1)}\right) \\ \vdots \\ C_2\left(\boldsymbol{A}^{(N)}\right) \odot C_2\left(\boldsymbol{B}^{(N)}\right) \end{bmatrix} \in \mathbb{C}^{\left(\sum_{n=1}^{N} C_{I_n}^2 C_{J_n}^2\right) \times C_R^2}.$$

If

$$\begin{cases} \boldsymbol{C} \text{ has full column rank,} \\ \boldsymbol{G} \text{ has full column rank,} \end{cases} \quad (11)$$

then the coupled rank of $\{\mathcal{X}^{(n)}\}$ is R and the coupled CPD of $\{\mathcal{X}^{(n)}\}$ is unique [29].

As in ordinary CPD, the uniqueness condition (11) is relatively easy to check and yet very powerful. It is also clear that more relaxed uniqueness conditions are obtained by taking the coupling into account. (Compare for instance condition (3) with condition (11)).

Furthermore, an extension of the SD method in [2] to the coupled CPD has been developed in [27], [32]. We emphasize that in the noise-free case the SD problem for coupled CPD can be solved via a GEVD.

III. Tensor based array processing

Consider R signals impinging on an array composed of I sensors such that the output of the ith sensor at the kth observation is

$$x_{ik} = \sum_{r=1}^{R} s_r(k - \tau_{ri}), \quad (12)$$

where τ_{ri} denotes the delay between the ith sensor and the rth source. The azimuth angle associated with the rth source is denoted by θ_r and is measured counterclockwise (see figure 1). Similarly, the elevation angle associated with the rth source is denoted by ϕ_r and is measured clockwise. The position of the ith sensor in cartesian coordinates is given by $\mathbf{p}_i = [x_i\ y_i\ z_i]^T$. Let us additionally assume that the sources are located in the

far-field and that the narrowband assumption holds (e.g. [33]). Under these assumptions the array response vector associated with the rth source can (approximately) be expressed as

$$\mathbf{a}_r = \left[e^{-i\omega_c\tau_{r1}} \ \ldots \ e^{-i\omega_c\tau_{rI}}\right]^T = \left[e^{-i\omega_c\mathbf{b}_r^T\mathbf{p}_1/c} \ \ldots \ e^{-i\omega_c\mathbf{b}_r^T\mathbf{p}_I/c}\right]^T \in \mathbb{C}^I,$$

where ω_c is the carrier frequency, c is the speed of propagation, $\mathbf{b}_r = [\sin(\phi_r)\cos(\theta_r),\ \sin(\phi_r)\sin(\theta_r),\ \cos(\phi_r)]^T$ is the bearing vector depicted in figure 1, and the product $\tau_{ri} = \mathbf{b}_r^T\mathbf{p}_i/c$ corresponds to the propagation delay associated with the ith sensor and the rth source. Assume that R sources are impinging on the sensor array and that K snapshots are available such that $\mathbf{s}_r \in \mathbb{C}^K$ denotes the signal vector associated with the rth source. Then the observed data matrix admits the factorization

$$\mathbf{X} = \mathbf{A}\mathbf{S}^T \in \mathbb{C}^{I\times K}, \quad \mathbf{A} = [\mathbf{a}_1, \ldots, \mathbf{a}_R], \ \mathbf{S} = [\mathbf{s}_1, \ldots, \mathbf{s}_R]. \quad (13)$$

In direction-of-arrival applications the goal is to estimate $\{\theta_r, \phi_r\}$ via $\mathbf{A}$, observing $\mathbf{X}$. On the other hand, in source separation the goal is to estimate $\mathbf{S}$, observing $\mathbf{X}$. For both problems, uniqueness conditions and algorithms need to be developed. To this end, either arrays with simple geometries or signals with predefined structures (statistical independence, finite alphabet, sparsity, etc.) are used. In this paper we focus on the former approach.

A. Basic CPD based array processing

Because of their simplicity, arrays composed of several displaced but identical subarrays are often considered in the literature (e.g. [22], [35], [34], [24], [36], [15]). More precisely, let x_{ijk} denote the output of the ith sensor of the jth subarray at the kth snapshot. Assume that J subarrays each composed of I sensors are used. Then the observed data tensor $\mathcal{X} \in \mathbb{C}^{I\times J\times K}$ admits the factorization

$$\mathcal{X} = \sum_{r=1}^{R} \mathbf{a}_r \circ \mathbf{d}_r \circ \mathbf{s}_r, \quad (14)$$

where $\mathbf{a}_r = \left[e^{-i\omega_c\mathbf{b}_r^T\mathbf{p}_1/c} \ \ldots \ e^{-i\omega_c\mathbf{b}_r^T\mathbf{p}_I/c}\right]^T \in \mathbb{C}^I$, $\mathbf{d}_r = \left[e^{-i\omega_c\mathbf{b}_r^T\mathbf{t}_1/c} \ \ldots \ e^{-i\omega_c\mathbf{b}_r^T\mathbf{t}_J/c}\right]^T \in \mathbb{C}^J$, and $\mathbf{s}_r \in \mathbb{C}^K$ denote the reference subarray, the displacement and signal vector associated with the rth source, respectively. In this case $\mathbf{p}_i$ denotes the position of the ith sensor in the reference subarray while $\mathbf{t}_j$ denotes the translation vector associated with the jth subarray.

Note that the I element subarray vector $\mathbf{a}_r$ is repeated J times and scaled according to the entries of $\mathbf{d}_r$:

$$\mathbf{a}_r\mathbf{d}_r^T = [\mathbf{a}_r(\mathbf{d}_r)_1 \ \ldots \ \mathbf{a}_r(\mathbf{d}_r)_J]. \quad (15)$$

The rank-1 structure in (15), reflecting the overall array geometry, explains why CPD is the proper model. We say that an array with a rank-1 structure of the form (15) enjoys a shift-invariance property. On the other hand, it is a notable limitation of the CPD approach is that to can only handle array configurations in which all subarrays are identical. More generally, an array may be composed of subarrays that have different configurations leading to multiple shift-invariance substructures. Such arrays will be discussed in sections IV and V.

The CPD variant where $J = 2$ corresponds to classical ESPRIT [22]. The case where $J > 2$ is known as Multiple Invariance ESPRIT (MI-ESPRIT) [35] and coincides with the CPD model (1). For the former case an algebraic method was proposed in [22]. For the case where $J > 2$ an algebraic method has more recently been proposed in [2]. This algorithm is here called the SD method. Hence, in the context of array processing the SD procedure can be interpreted as an algebraic MI-ESPRIT method.

B. Constrained CPD based array processing

In practice, the inter-element spacing of the sensors in the reference subarray may be constant ($\{\mathbf{a}_r\}$ in (14) are Vandermonde vectors) or the subarrays may be uniformly displaced ($\{\mathbf{d}_r\}$ in (14) are Vandermonde vectors). From relation (14) we now obtain the constrained decomposition

$$\mathbf{X}_{(1)} = (\mathbf{A} \odot \mathbf{D})\,\mathbf{S}^T \in \mathbb{C}^{IJ\times K}. \quad (16)$$

in which $\mathbf{A}$ or $\mathbf{D}$ are Vandermonde. The simplest example is a Uniform Linear Array (ULA) along the x-axis where $\mathbf{a}_r = \left[1,\ x_r,\ \ldots,\ x_r^{I-1}\right]^T$ in which $x_r = e^{-i\omega_c d_x \sin(\phi_r)\cos(\theta_r)/c}$ and d_x denotes the inter-element spacing along the x-axis [28].

For the URA in figure 2 (left), we have $\mathbf{a}_r = \left[1,\ x_r,\ \ldots,\ x_r^{I-1}\right]^T$ in which $x_r = e^{-i\omega_c d_x \sin(\phi_r)\cos(\theta_r)/c}$ and d_x denotes the inter-element spacing along the x-axis, and $\mathbf{d}_r = \left[1,\ y_r,\ \ldots,\ y_r^{J-1}\right]^T$ in which $y_r = e^{-i\omega_c d_y \sin(\phi_r)\sin(\theta_r)/c}$ and d_y denotes the inter-element spacing along the y-axis. From (14) we now obtain a constrained CPD in which both $\mathbf{A}$ and $\mathbf{D}$ in (16) are Vandermonde. This can also be interpreted as a two-dimensional (2D) Harmonic Retrieval (HR) problem. A link between 2D HR and coupled CPD was proposed in [30]. Based on the connection between 2D HR and coupled CPD, dedicated uniqueness conditions and algorithms for URA (and related HR) problems were developed in [30].

C. CPD based array processing in the case of real signals

We have already mentioned that CPD problems with two Vandermonde factor matrices can be addressed as coupled CPD problems. Here we establish a link between the coupled CPD and CPD based array processing problems that involve a real factor matrix. To make it more concrete, we consider a wireless communication system equipped with $I \geq 2$ electromagnetic VSAs [19] in which the signal matrix $\mathbf{S} \in \mathbb{C}^{K\times R}$ admits the factorization $\mathbf{S} = \mathbf{S}_0\mathbf{D}_\mathbf{S}$, where $\mathbf{S}_0 \in \mathbb{R}^{K\times R}$ is real and $\mathbf{D}_\mathbf{S} = D_1\left([e^{i\varphi_1}, \ldots, e^{i\varphi_R}]\right)$ contains the phase shifts in which $\varphi_r \in \mathbb{R}$. A simple example is BPSK transmitted data sequences. Assume additionally that the impinging signals are narrowband and that the emitters are located

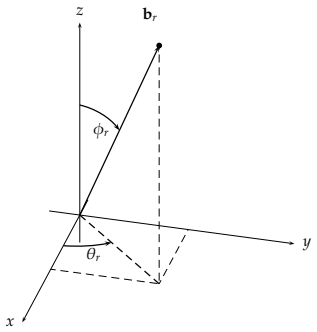

Fig. 1. Bearing vector $\mathbf{b}_r$ associated the rth source in which θ_r and ϕ_r denote the azimuth and elevation angle, respectively.

in the far-field. Let us apply the CPD model presented in [10] where $\mathbf{d}_r \in \mathbb{C}^6$ is of the form

$$\mathbf{d}_r = \begin{bmatrix} -\sin\theta_r & -\cos\theta_r \sin\phi_r \\ \cos\theta_r & -\sin\theta_r \sin\phi_r \\ 0 & \cos\phi_r \\ -\cos\theta_r \sin\phi_r & \sin\theta_r \\ -\sin\theta_r \sin\phi_r & -\cos\theta_r \\ \cos\phi_r & 0 \end{bmatrix} \mathbf{p}(\alpha_r, \beta_r), \quad (17)$$

in which $\mathbf{p}(\alpha_r, \beta_r) = \begin{bmatrix} \cos\alpha_r & \sin\alpha_r \\ -\sin\alpha_r & \cos\alpha_r \end{bmatrix} \begin{bmatrix} \cos\beta_r \\ i \cdot \sin\beta_r \end{bmatrix}$ and both the azimuth and elevation angles are measured counter-clockwise and the pair (α_r, β_r) describes the polarization state of the rth impinging signal [19]. Define $\mathcal{Y} \in \mathbb{C}^{I \times J \times K}$ as follows $y_{ijk} = x^*_{ijk}$. From (14) we obtain the coupled CPD of $\{\mathcal{X}, \mathcal{Y}\}$ with matrix representation

$$\begin{bmatrix} \mathbf{X}_{(1)} \\ \mathbf{Y}_{(1)} \end{bmatrix} = \begin{bmatrix} (\mathbf{A} \odot \mathbf{D})\mathbf{D}_\mathbf{S} \\ (\mathbf{A}^* \odot \mathbf{D}^*)\mathbf{D}^*_\mathbf{S} \end{bmatrix} \mathbf{S}_0^T. \quad (18)$$

The link between CPD with a real factor matrix and coupled CPD leads to improved uniqueness conditions and algorithms. For instance, assume that $I = 3$ VSAs are used such that $\mathbf{a}_r = \left[1, x_r^{d_2}, x_r^{d_3}\right]^T \in \mathbb{C}^3$ where $x_r = e^{-i\omega_c \cos(\phi_r)\cos(\theta_r)/c}$. Assume also that $d_2 = c/\omega_c$ and $d_3 = 7c/2\omega_c$, $\mathbf{d}_r \in \mathbb{C}^6$ is given by (17) in which $J = 6$, and $\mathbf{S}_0 \in \mathbb{R}^{K \times R}$ is real and has full column rank ($K \geq R$). By only capitalizing on the CPD structure of $\mathcal{X}$, Theorem II.1 yields the bound $R \leq 10$. On the other hand, by exploiting the coupled CPD structure of $\{\mathcal{X}, \mathcal{Y}\}$, Theorem II.3 tells us that we can relax the bound to $R \leq 13$. Note also that the factors can be computed via the SD procedure for coupled CPD.

IV. New results for arrays with multiple shift-invariance structures based on the coupled CPD

The main limitation of the standard tensor-based methods for array processing is that the observed data must admit a (constrained) CPD interpretation of the form (14). To alleviate this problem, we suggest to model data received by an array that has N shift-invariance structures by a coupled CPD of the form

$$\mathbb{C}^{I_n \times J_n \times K} \ni \mathcal{X}^{(n)} = \sum_{r=1}^{R} \mathbf{a}_r^{(n)} \circ \mathbf{d}_r^{(n)} \circ \mathbf{s}_r, \quad n \in \{1, \ldots, N\}, \quad (19)$$

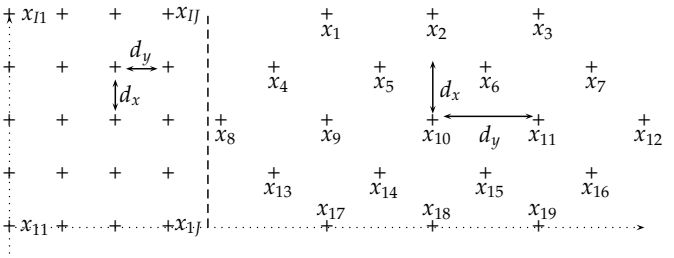

Fig. 2. Uniform rectangular shaped array (left) and hexagonal shaped array (right) where '+' represents an antenna element.

where N denotes the number of shift-invariance structures that have been taken into account, and where $\mathbf{a}_r^{(n)} \in \mathbb{C}^{I_n}$ and $\mathbf{d}_r^{(n)} \in \mathbb{C}^{J_n}$ denote the nth reference subarray response vector and its associated displacement vector, respectively.

For convenience of presentation, we will mainly focus on very regular array geometries with multiple shift-invariance structures. We only consider 2D planar arrays ($z_r = 0$ in (13)) and linearly independent impinging signals. The extension to three-dimensional (3D) arrays ($z_r \neq 0$ in (13)) is completely analogous, i.e., the coupled CPD framework can handle any N-dimensional array as long as it contains shift-invariance structures. The results can also be extended to linearly dependent signals. We stress that the coupled matrix/tensor based array processing framework implemented here via the coupled CPD model (19) also works for irregular array geometries provided that they contain shift-invariance structures.

The section is organized as follows. In subsections IV-A and IV-B we consider so-called centro-symmetric and asymmetric arrays. The reason for this distinction is that in the former case we can apply FBA in a preprocessing step while in the latter case this is not possible (at least not in a straightforward manner).

A. Centro-symmetric regular arrays

Let us first explain how the coupled CPD model (19) can be used in the case of centro-symmetric arrays (i.e., arrays that are symmetric around their "epicenter") with multiple shift-invariance structures.

1) Hexagonal Array (HA): Consider the nineteen element HA depicted in figure 2 (right) and adapted from [37]. The inter-element spacings are $d_y = \lambda/2$ and $d_x = \sqrt{3}\lambda/4$ in which $\lambda = 2\pi c/\omega_c$. Note that the HA cannot be fully described by means of a CPD. However, it was observed in [37] that this HA consists of subarrays each composed of fourteen sensors that enjoy a shift-invariance property. As our contribution, we will explain how to exploit the latter overall structure.

Let the reference sensor be x_{10}. The columns of $\mathbf{A}$ in (13) take the form $\mathbf{a}_r = [\mathbf{b}_r^{(1)}, \mathbf{b}_r^{(2)}, \mathbf{b}_r^{(3)}, \mathbf{b}_r^{(2)*}, \mathbf{b}_r^{(1)*}]^T$ where $\mathbf{b}_r^{(1)} = e^{i\pi\sqrt{3}x_r}[e^{-i\pi y_r}, 1, e^{i\pi y_r}]$, $\mathbf{b}_r^{(2)} = e^{i\pi\frac{\sqrt{3}}{2}x_r}[e^{-i\pi\frac{3y_r}{2}}, e^{-i\pi\frac{y_r}{2}}, e^{i\pi\frac{y_r}{2}}, e^{-i\pi\frac{3y_r}{2}}]$ and $\mathbf{b}_r^{(3)} = [e^{-i\pi 2y_r}, e^{-i\pi y_r}, 1, e^{i\pi y_r}, e^{i\pi 2y_r}]$ with $x_r = \sin(\phi_r)\cos(\theta_r)$ and $y_r = \sin(\phi_r)\sin(\theta_r)$.

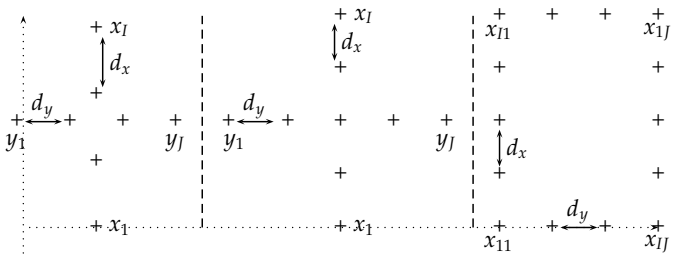

Fig. 3. Cross-shaped arrays (left and middle) and frame-shaped array (right) where '+' represents an antenna element.

FBA produces the augmented matrix

$$\mathbf{Y} = [\mathbf{X}, \mathbf{J}_{19}\mathbf{X}^*] = \mathbf{A}\left[\mathbf{S}^T, \mathbf{S}^H\right] \in \mathbb{C}^{19\times 2K}, \tag{20}$$

where the property $\mathbf{J}_{19}\mathbf{A}^* = \mathbf{A}$ was taken into account. Define the $14 \times 2K$ matrices

$$\mathbf{Y}^{(1)} = \mathbf{Y}([1:11,13,14,15],:), \mathbf{Y}^{(3)} = \mathbf{Y}([5,6,7,9:19],:),$$
$$\mathbf{Y}^{(2)} = \mathbf{Y}([2,3,5,6,7,9,10,11,12,14,15,16,18,19],:),$$
$$\mathbf{Y}^{(4)} = \mathbf{Y}([1,2,4,5,6,8,9,10,11,13,14,15,17,18],:).$$

Define $\mathbf{A}^{(n)}$ similarly (e.g. $\mathbf{A}^{(1)} = \mathbf{A}([1:11,13,14,15],:)$). Define also

$$\mathbf{D}^{(1)} = \begin{bmatrix} 1 & \cdots & 1 \\ m_1 & \cdots & m_R \end{bmatrix}, \mathbf{D}^{(2)} = \begin{bmatrix} 1 & \cdots & 1 \\ n_1 & \cdots & n_R \end{bmatrix},$$

where $m_r = e^{-i\pi\sqrt{3}x_r/2}e^{i\pi y_r/2}$ and $n_r = e^{-i\pi y_r}$. The following shift-invariance structures can be observed

$$\mathbf{A}^{(1)}D_2(\mathbf{D}^{(1)}) = \mathbf{A}^{(3)}, \quad \text{and} \quad \mathbf{A}^{(2)}D_2(\mathbf{D}^{(2)}) = \mathbf{A}^{(4)},$$

This motivates the construction of tensors $\{\mathcal{Z}^{(1)}, \mathcal{Z}^{(2)}\}$ of which the matrix representation admits the coupled decomposition

$$\begin{bmatrix} \mathbf{Z}^{(1)} \\ \mathbf{Z}^{(2)} \end{bmatrix} = (\mathbf{I}_2 \otimes \mathbf{P}) \begin{bmatrix} \mathbf{Y}^{(1)} \\ \mathbf{Y}^{(3)} \\ \hline \mathbf{Y}^{(2)} \\ \mathbf{Y}^{(4)} \end{bmatrix} = \begin{bmatrix} \mathbf{A}^{(1)} \odot \mathbf{D}^{(1)} \\ \mathbf{A}^{(2)} \odot \mathbf{D}^{(2)} \end{bmatrix} \left[\mathbf{S}^T, \mathbf{S}^H\right], \tag{21}$$

where $\mathbf{P}$ is the permutation matrix such that $\mathbf{P}(\mathbf{D}^{(n)} \odot \mathbf{A}^{(n)}) = \mathbf{A}^{(n)} \odot \mathbf{D}^{(n)}$. We exploited that $\mathbf{A}^{(n)} \in \mathbb{C}^{14\times R}$ and $\mathbf{D}^{(n)} \in \mathbb{C}^{2\times R}$ for all $n \in \{1,2\}$. From (21) it is clear that the factor matrices can be retrieved via a coupled CPD. The results are readily extended to other HAs. The coupled CPD approach leads to improved identifiability for HAs. As an example, if we only exploit the CPD structure of the nineteen element HA, say $\mathcal{Z}^{(1)}$, then from Theorem II.1 we obtain the bound $R \leq 14$. Thanks to Theorem II.3 the coupled CPD structure of $\{\mathcal{Z}^{(1)}, \mathcal{Z}^{(2)}\}$ relaxes the bound to $R \leq 16$. The coupled CPD of $\{\mathcal{Z}^{(1)}, \mathcal{Z}^{(2)}\}$ can also be computed via MHR-ESPRIT methods [30].

2) Cross-shaped Array (CA): Consider the CA in figure 3 (middle), composed of a horizontal and vertical array (e.g. [11]). It is assumed that I and J are odd numbers such that the horizontal and vertical arrays share one sensor. Since the horizontal and vertical arrays are not shifted versions of each other, it is crucial in our framework that the individual arrays have shift-invariance properties. Here we consider the simple case where both the horizontal and vertical arrays are ULAs. Let us choose the sensor located at the "epicenter" of the CA as the reference sensor. The observed data can be stored into the matrices $\mathbf{X}^{(1)}$ and $\mathbf{X}^{(2)}$, where $x_{ik}^{(1)}$ and $x_{ik}^{(2)}$ denote the outputs of the vertical and horizontal arrays at snapshot k, respectively. The narrowband and far-field assumptions imply that

$$\mathbf{X}^{(1)} = \mathbf{B}^{(1)}\mathbf{S}^T, \quad \mathbf{X}^{(2)} = \mathbf{B}^{(2)}\mathbf{S}^T, \tag{22}$$

where $\mathbf{b}_r^{(1)} = [x_r^{(1-I)/2}, \ldots, x_r^{(I-1)/2}]$ in which $x_r = e^{-i\omega_c d_x \sin(\phi_r)\cos(\theta_r)/c}$, $\mathbf{b}_r^{(2)} = [y_r^{(1-J)/2}, \ldots, y_r^{(J-1)/2}]$ in which $y_r = e^{-i\omega_c d_y \sin(\phi_r)\sin(\theta_r)/c}$, and $\mathbf{S} \in \mathbb{C}^{K\times R}$ is the collected signal matrix. FBA yields

$$\begin{bmatrix} \mathbf{Y}^{(1)} \\ \mathbf{Y}^{(2)} \end{bmatrix} = \begin{bmatrix} \mathbf{X}^{(1)} & \mathbf{J}_I\mathbf{X}^{(1)*} \\ \mathbf{X}^{(2)} & \mathbf{J}_J\mathbf{X}^{(2)*} \end{bmatrix} = \begin{bmatrix} \mathbf{B}^{(1)} \\ \mathbf{B}^{(2)} \end{bmatrix} \left[\mathbf{S}^T, \mathbf{S}^H\right], \tag{23}$$

where we exploited the centro-symmetry in $\mathbf{J}_I\mathbf{B}^{(1)*} = \mathbf{B}^{(1)}$ and $\mathbf{J}_J\mathbf{B}^{(2)*} = \mathbf{B}^{(2)}$. Using spatial smoothing (see [30] for details) we obtain tensors $\{\mathcal{Z}^{(1)}, \mathcal{Z}^{(2)}\}$ of which the matrix representation admits the coupled decomposition

$$\begin{bmatrix} \mathbf{Z}^{(1)} \\ \mathbf{Z}^{(2)} \end{bmatrix} = \begin{bmatrix} \mathbf{A}^{(1)} \odot \mathbf{D}^{(1)} \\ \mathbf{A}^{(2)} \odot \mathbf{D}^{(2)} \end{bmatrix} \left[\mathbf{S}^T, \mathbf{S}^H\right], \tag{24}$$

where

$$\mathbf{a}_r^{(1)} = \left[x_r^{(2-I)/2}, \ldots, x_r^{(I-2)/2}\right]^T, \quad \mathbf{d}_r^{(1)} = \left[x_r^{-\frac{1}{2}}, x_r^{\frac{1}{2}}\right]^T,$$
$$\mathbf{a}_r^{(2)} = \left[y_r^{(2-J)/2}, \ldots, y_r^{(J-2)/2}\right]^T, \quad \mathbf{d}_r^{(2)} = \left[y_r^{-\frac{1}{2}}, y_r^{\frac{1}{2}}\right]^T.$$

From (24) it is clear that CA problems involving shift-invariant subarrays can be addressed as coupled CPD problems. This leads to improved uniqueness conditions. As an example, consider the case where $I = J = 5$ and $K \geq R$. If we only exploit the CPD structure of, say $\mathcal{Z}^{(1)}$, then from Theorem II.1 we obtain the bound $R \leq 4$. Thanks to Theorem II.3 the coupled CPD structure of $\{\mathcal{Z}^{(1)}, \mathcal{Z}^{(2)}\}$ relaxes the bound to $R \leq 5$. Again, the coupled CPD of $\{\mathcal{Z}^{(1)}, \mathcal{Z}^{(2)}\}$ can be computed via the MHR-ESPRIT methods [30].

Let us now briefly consider the case where I and J are even numbers. Let us choose the left-middle sensor in the horizontal ULA as the reference sensor. By exploiting the phase indeterminacy of the problem (due to the delay between the source and the reference sensor) we can choose the centre of the "x-y plane" as the phase reference center. Consider the following phase-centered variant of (22):

$$\mathbf{X}^{(1)} = \mathbf{B}^{(1)}\mathbf{D}\mathbf{S}^T, \quad \mathbf{X}^{(2)} = \mathbf{B}^{(2)}\mathbf{D}\mathbf{S}^T,$$

where again $\mathbf{b}_r^{(1)} = [x_r^{(1-I)/2}, \ldots, x_r^{(I-1)/2}]$ and $\mathbf{b}_r^{(2)} = [y_r^{(1-I)/2}, \ldots, y_r^{(I-1)/2}]$ while now $\mathbf{D} = D_1([y_1^{1/2}, \ldots, y_R^{1/2}])$. Following the same procedure as before we obtain (24) provided that $[\mathbf{S}^T, \mathbf{S}^H]$ is replaced by $[\mathbf{D}\mathbf{S}^T, \mathbf{D}^*\mathbf{S}^H]$.

3) Frame-shaped Array (FA): A simple generalization of the CA is the FA composed of two horizontal and vertical arrays as depicted in figure 3 (right). The difference between the CA and the FA is that in the latter configuration there is a shift-invariance structure between the involved horizontal and vertical arrays. Consequently, in a FA the individual subarrays are not required to be shift-invariant; this case is briefly discussed in subsection IV-B2. Here we consider the simple case where the horizontal and vertical arrays are ULAs and explain how this additional ULA structure can be taken into account.

Build the FA observation matrices $\mathbf{X}^{(1)} \in \mathbb{C}^{2I\times K}$ with columns $\mathbf{x}_k^{(1)} = [x_{11k},\ldots,x_{I1k},x_{1Jk},\ldots,x_{IJk}]^T$ and $\mathbf{X}^{(2)} \in \mathbb{C}^{2J\times K}$ with columns $\mathbf{x}_k^{(2)} = [x_{11k},\ldots,x_{1Jk},x_{I1k},\ldots,x_{IJk}]^T$, where x_{ijk} denotes the output of sensor x_{ij} at the kth snapshot and with indexing as indicated in figure 3 (right). The matrices $\mathbf{X}^{(1)}$ and $\mathbf{X}^{(2)}$ admit the factorizations

$$\mathbf{X}^{(1)} = \left(\mathbf{B}^{(1)} \odot \mathbf{C}^{(1)}\right)\mathbf{S}^T, \quad \mathbf{X}^{(2)} = \left(\mathbf{B}^{(2)} \odot \mathbf{C}^{(2)}\right)\mathbf{S}^T, \qquad (25)$$

where

$$\begin{aligned} \mathbf{b}_r^{(1)} &= [1\ x_r\ \ldots\ x_r^{(I-1)}]^T, \quad \mathbf{c}_r^{(1)} = [1\ y_r^{(J-1)}]^T, \\ \mathbf{b}_r^{(2)} &= [1\ y_r\ \ldots\ y_r^{(J-1)}]^T, \quad \mathbf{c}_r^{(2)} = [1\ x_r^{(I-1)}]^T, \end{aligned}$$

in which $x_r = e^{-i\omega_c d_x \sin(\phi_r)\cos(\theta_r)/c}$ where d_x denotes the inter-element spacing along the x-axis, and $y_r = e^{-i\omega_c d_y \sin(\phi_r)\sin(\theta_r)/c}$ where d_y denotes the inter-element spacing along the y-axis. FBA produces the augmented matrix

$$\begin{bmatrix} \mathbf{Y}^{(1)} \\ \mathbf{Y}^{(2)} \end{bmatrix} = \begin{bmatrix} \mathbf{X}^{(1)} & \mathbf{J}_{I2}\mathbf{X}^{(1)*} \\ \mathbf{X}^{(2)} & \mathbf{J}_{J2}\mathbf{X}^{(2)*} \end{bmatrix} = \begin{bmatrix} \mathbf{B}^{(1)} \odot \mathbf{C}^{(1)} \\ \mathbf{B}^{(2)} \odot \mathbf{C}^{(2)} \end{bmatrix}\left[\mathbf{S}^T, \mathbf{D}\mathbf{S}^H\right],$$

where $\mathbf{D} = D_1([x_1^{-(I-1)}y_1^{-(J-1)},\ldots,x_R^{-(I-1)}y_R^{-(J-1)}])$. Using spatial smoothing we obtain tensors $\{\mathcal{Z}^{(1)},\mathcal{Z}^{(2)}\}$ of which the matrix representation admits the coupled decomposition

$$\begin{bmatrix} \mathbf{Z}^{(1)} \\ \mathbf{Z}^{(2)} \end{bmatrix} = \begin{bmatrix} \mathbf{A}^{(1)} \odot \mathbf{D}^{(1)} \\ \mathbf{A}^{(2)} \odot \mathbf{D}^{(2)} \end{bmatrix}\left[\mathbf{S}^T, \mathbf{D}\mathbf{S}^H\right], \qquad (26)$$

where $\mathbf{A}^{(1)} = \underline{\mathbf{B}}^{(1)} \odot \mathbf{C}^{(1)}$, $\mathbf{A}^{(2)} = \underline{\mathbf{B}}^{(2)} \odot \mathbf{C}^{(2)}$ and

$$\mathbf{D}^{(1)} = \begin{bmatrix} 1 & \cdots & 1 \\ x_1 & \cdots & x_R \end{bmatrix}, \quad \mathbf{D}^{(2)} = \begin{bmatrix} 1 & \cdots & 1 \\ y_1 & \cdots & y_R \end{bmatrix}.$$

Note that in (26) we have exploited both the shift-invariance structures within and between the horizontal and vertical arrays. The structure in (26) leads to improved uniqueness conditions. As an example, consider the case where $I = J = 5$ and $K \geq R$. If we only exploit the CPD structure of, say $\mathcal{Z}^{(1)}$, then from Theorem II.1 we obtain the bound $R \leq 8$. Thanks to Theorem II.3 the coupled CPD structure of $\{\mathcal{Z}^{(1)},\mathcal{Z}^{(2)}\}$ relaxes the bound to $R \leq 10$. Again, the coupled CPD of $\{\mathcal{Z}^{(1)},\mathcal{Z}^{(2)}\}$ can be computed via MHR-ESPRIT methods [30].

B. Asymmetric arrays

Many array configurations are not symmetric around their "epicenter". We call them asymmetric. In subsection IV-B1 we first consider the case of superimposed arrays with no apparent shift-invariance structure among them. For simplicity, we limit the exposition to ULAs. Next, in subsections IV-B2 and IV-B3 we consider asymmetric arrays composed of superimposed arrays with shift-invariance structures between them.

1) Arrays composed of several linear arrays: Several proposed array configurations are based on the combination of ULAs. Some well-known examples are V-Shaped Arrays (VAs) [9], [8] and L-Shaped Arrays (LAs) [12]. Here we consider the Y-shaped Array (YA) in figure 5 (middle). The YA is clearly composed of three ULAs. Assume that K snapshots are available. Let us choose the sensor denoted by $x_1 = y_1 = z_1$ in figure 5 (middle) as the reference sensor. The outputs of the three ULAs can be stacked into the matrices $\mathbf{X}^{(1)}$, $\mathbf{X}^{(2)}$ and $\mathbf{X}^{(3)}$ according to $(\mathbf{X}^{(1)})_{ik} = x_{ik}$, $(\mathbf{X}^{(2)})_{ik} = y_{ik}$ and $(\mathbf{X}^{(3)})_{ik} = z_{ik}$, where the index k denotes the snapshot number. This leads to the matrix factorizations

$$\mathbf{X}^{(1)} = \mathbf{B}^{(1)}\mathbf{S}^T, \quad \mathbf{X}^{(2)} = \mathbf{B}^{(2)}\mathbf{S}^T, \quad \mathbf{X}^{(3)} = \mathbf{B}^{(3)}\mathbf{S}^T, \qquad (27)$$

where $\mathbf{S} \in \mathbb{C}^{K\times R}$ is the collected signal matrix and

$$\begin{aligned} \mathbf{b}_r^{(1)} &= [1, x_r, \ldots, x_r^{(I_1-1)}], \quad x_r = e^{-i\omega_c d_x \sin(\phi_r)\cos(\theta_r-\alpha)/c}, \\ \mathbf{b}_r^{(2)} &= [1, y_r, \ldots, y_r^{(I_2-1)}], \quad y_r = e^{-i\omega_c d_y \sin(\phi_r)\cos(\theta_r-\beta)/c}, \\ \mathbf{b}_r^{(3)} &= [1, z_r, \ldots, z_r^{(I_3-1)}], \quad z_r = e^{-i\omega_c d_z \sin(\phi_r)\cos(\theta_r-\gamma)/c}, \end{aligned}$$

in which α, β and γ denote the angles between the "x axis" and the individual ULA "axes". Using spatial smoothing on the matrices $\{\mathbf{X}^{(n)}\}$ we obtain tensors $\{\mathcal{Y}^{(n)}\}$ of which the matrix representation admits the coupled decomposition

$$\begin{bmatrix} \mathbf{Y}^{(1)} \\ \mathbf{Y}^{(2)} \\ \mathbf{Y}^{(3)} \end{bmatrix} = \begin{bmatrix} \mathbf{A}^{(1)} \odot \mathbf{D}^{(1)} \\ \mathbf{A}^{(2)} \odot \mathbf{D}^{(2)} \\ \mathbf{A}^{(3)} \odot \mathbf{D}^{(3)} \end{bmatrix}\mathbf{S}^T, \qquad (28)$$

where $\mathbf{A}^{(n)} = \underline{\mathbf{B}}^{(n)}$ and $\mathbf{D}^{(n)} = \mathbf{B}^{(n)}(1:2,:)$. Clearly (28) corresponds to a coupled CPD problem of the form (19). The CPD structure of $\{\mathcal{Y}^{(n)}\}$ is thanks to the ULA geometry. On the other hand, the coupling is due to the fact that $\mathbf{S}$ is the same for the three subarrays. The coupled CPD structure leads to improved uniqueness conditions for the YA. Furthermore, the SD method for coupled CPD in [32] can be used for the actual computation.

The VA in [9], [8] is just a YA with $I_3 = 1$. Similarly, the LA in [12] is also just a special case of the YA. For instance, by setting $I_3 = 1$, $\alpha = 0$ and $\beta = \frac{\pi}{2}$ we obtain an array composed of two perpendicular ULAs. The result is also valid for other array geometries based on the superposition of linear arrays, e.g., the right-triangular shaped array in [12].

2) Irregular arrays: Here we briefly demonstrate that the coupled CPD model (19) applies also to irregular arrays provided they are embedded with shift-invariance structures. An hypothetical irregular array with shift-invariance structures is depicted in figure 4. Let us revisit the FA from subsection IV-A3 where now the individual horizontal and vertical arrays do not contain any shift-invariance structure. As an example, let the columns of

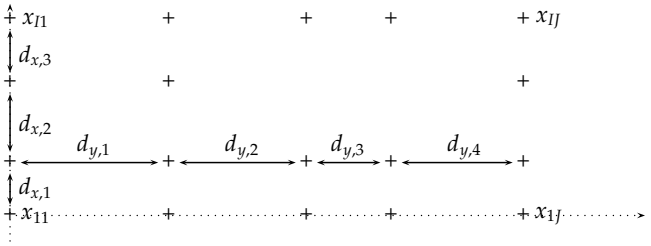

Fig. 4. An hypothetical irregular array with shift-invariance structures where '+' represents an antenna element.

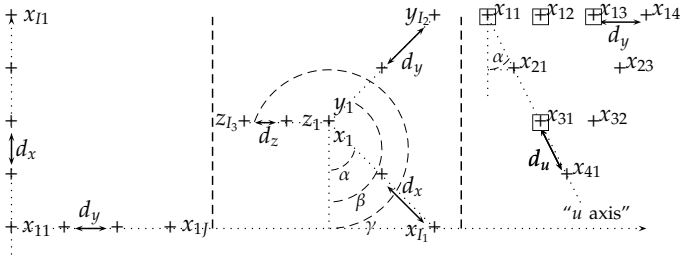

Fig. 5. L-shaped array (left), Y-shaped array (middle) and triangular-shaped array (right) where '+' represents an antenna element.

$\mathbf{B}^{(n)}$ and $\mathbf{C}^{(n)}$ in (25) be of the form

$$\begin{aligned}\mathbf{b}_r^{(1)} &= [1, x_r^{m_1}, \ldots, x_r^{m_{I-1}}]^T, \quad \mathbf{c}_r^{(1)} = [1, y_r^{n_{J-1}}]^T,\\ \mathbf{b}_r^{(2)} &= [1, y_r^{n_1}, \ldots, y_r^{n_{J-1}}]^T, \quad \mathbf{c}_r^{(2)} = [1, x_r^{m_{I-1}}]^T,\end{aligned}$$

in which m_i and n_j denote the spacings between the sensors and the reference sensor along the x-axis and y-axis, respectively. Due to the shift-invariance structure between the horizontal and vertical subarrays we still obtain a coupled CPD problem of the form (25).

3) Triangular-shaped Array (TA): Consider the nine-element TA depicted in figure 5 (right). Let x_{mnk} denote the output of sensor x_{mn} at snapshot k. Then the kth column of $\mathbf{X}$ and the rth column of $\mathbf{A}$ in (13) are given by

$$\begin{aligned}\mathbf{x}_k &= [x_{11k}, x_{12k}, x_{13k}, x_{14k}, x_{21k}, x_{23k}, x_{31k}, x_{32k}, x_{41k}]^T,\\ \mathbf{a}_r &= \left[1, y_r, y_r^2, y_r^3, x_r, x_r y_r^2, x_r^2, x_r^2 y_r, x_r^3\right]^T,\end{aligned}$$

where $y_r = e^{-i\frac{\omega_c}{c} d_y \sin(\theta_r)\sin(\phi_r)}$ and $x_r = e^{-i\frac{\omega_c}{c} d_u \cos(\theta_r - \alpha)\sin(\phi_r)}$ in which α denotes the angle between the "x axis" and the "u axis", see figure 5 (right). At first sight one may view the TA as three superimposed ULAs each composed of three sensors. However, we observe that this TA contains three subarrays (one of the four-element subarrays is highlighted in the figure by squared boxes) each composed of four sensors that also enjoy a shift-invariance property. More precisely, the TA has the following three shift-invariance structures:

$$\mathbf{a}_r^{(1)} := \mathbf{a}_r([1,2,3,\ 7]) = \mathbf{a}_r([2,3,4,\ 8])\, y_r^{-1}, \tag{29}$$

$$\mathbf{a}_r^{(2)} := \mathbf{a}_r([1,5,7,\ 3]) = \mathbf{a}_r([5,7,9,\ 7])\, x_r^{-1}, \tag{30}$$

$$\mathbf{a}_r^{(3)} := \mathbf{a}_r([4,6,8,\ 2]) = \mathbf{a}_r([6,8,9,\ 5])\, (x_r/y_r)^{-1}. \tag{31}$$

This motivates the construction of the tensors $\mathcal{X}^{(1)}$, $\mathcal{X}^{(2)}$ and $\mathcal{X}^{(3)}$ with matrix representation

$$\begin{aligned}\mathbf{X}^{(1)} &= [\mathbf{X}([1,2,3,\ 7],:)^T, \mathbf{X}([2,3,4,\ 8],:)^T]^T,\\ \mathbf{X}^{(2)} &= [\mathbf{X}([1,5,7,\ 3],:)^T, \mathbf{X}([5,7,9,\ 7],:)^T]^T,\\ \mathbf{X}^{(3)} &= [\mathbf{X}([4,6,8,\ 2],:)^T, \mathbf{X}([6,8,9,\ 5],:)^T]^T.\end{aligned}$$

The matrix representation of the tensors $\{\mathcal{X}^{(1)}, \mathcal{X}^{(2)}, \mathcal{X}^{(3)}\}$ admits the coupled decomposition

$$\mathbf{Y} = (\mathbf{I}_3 \otimes \mathbf{P}) \begin{bmatrix} \mathbf{X}^{(1)} \\ \mathbf{X}^{(2)} \\ \mathbf{X}^{(3)} \end{bmatrix} = \begin{bmatrix} \mathbf{A}^{(1)} \odot \mathbf{D}^{(1)} \\ \mathbf{A}^{(2)} \odot \mathbf{D}^{(2)} \\ \mathbf{A}^{(3)} \odot \mathbf{D}^{(3)} \end{bmatrix} \mathbf{S}^T, \tag{32}$$

where $\mathbf{P}$ is the permutation matrix such that $\mathbf{P}(\mathbf{D}^{(n)} \odot \mathbf{A}^{(n)}) = \mathbf{A}^{(n)} \odot \mathbf{D}^{(n)}$, the columns of $\mathbf{A}^{(1)}$, $\mathbf{A}^{(2)}$, $\mathbf{A}^{(3)}$ are of the form (29)–(31) and the columns of $\mathbf{D}^{(1)}$, $\mathbf{D}^{(2)}$, $\mathbf{D}^{(3)}$ are given by $\mathbf{d}_r^{(1)} = \begin{bmatrix} 1 \\ y_r \end{bmatrix}$, $\mathbf{d}_r^{(2)} = \begin{bmatrix} 1 \\ x_r \end{bmatrix}$ and $\mathbf{d}_r^{(3)} = \begin{bmatrix} 1 \\ x_r/y_r \end{bmatrix}$, respectively. Note that if we only exploit the CPD structure of, say $\mathcal{X}^{(1)}$, then from Theorem II.1 we obtain the upper bound $R \leq 4$. By exploiting the coupled CPD structure of $\{\mathcal{X}^{(1)}, \mathcal{X}^{(2)}, \mathcal{X}^{(3)}\}$, Theorem II.3 relaxes the bound to $R \leq 6$. Note also that the SD method for coupled CPD in [32] can be used for the computation.

The result can in an analogous way be extended to larger TAs such as those considered in [14]. The method is also valid for other related arrays. We mention the octagon shaped framed array in [12] which can be modeled as a coupled CPD of the form (19) with $N = 4$ shift-invariance structures.

V. Vector-sensor array processing via coupled CPD

Consider R far-field wideband signals impinging on an array composed of I vector-sensors (e.g. [19], [18]). The delay between emitter r and the ith vector-sensor is denoted by $\tau_{i,r} \in \mathbb{R}$. The output of the ith vector-sensor at the kth observation is

$$y_{il}(k) = \sum_{r=1}^{R} d_{lr} s_r(k - \tau_{i,r}), \tag{33}$$

where $\mathbf{d}_r \in \mathbb{C}^L$ is a diversity vector. The diversity can for instance be related to the use of polarization [6], [20] or velocity [1], [16], [38] sensitive sensors. Let us choose the first sensor indexed by $i = 1$ as the reference sensor. Since the impinging signals are not narrowband, the observation model in (13) does not apply anymore. Instead we first partition the observed data into M frames each lasting F samples such that the mth frame is given by $\mathbf{y}^{(i,m,l)} = [y_{il}((m-1)F+1), \ldots, y_{il}(mF)]^T$. Next, we transform the data into the frequency domain by means of the DFT matrix $\mathbf{W} \in \mathbb{C}^{F \times F}$ with $(\mathbf{W})_{gh} = e^{-i\cdot 2\pi \cdot g \cdot h/F}$ as follows $\mathbf{z}^{(i,m,l)} = \mathbf{W}\mathbf{y}^{(i,m,l)}$. Finally, we stack the vectors $\{\mathbf{z}^{(i,m,l)}\}$ into $\mathcal{Z}^{(f)} \in \mathbb{C}^{I \times M \times L}$ as follows $z^{(f)}_{i,m,l} = z^{(i,m,l)}_f$. The tensors $\mathcal{Z}^{(f)}$ admit the factorizations

$$\mathcal{Z}^{(f)} = \sum_{r=1}^{R} \mathbf{a}_r^{(f)} \circ \mathbf{s}_r^{(f)} \circ \mathbf{d}_r, \quad f \in \{1, \ldots, F\}, \tag{34}$$

where $\mathbf{s}_r^{(f)} \in \mathbb{C}^M$ denotes the rth signal vector at frequency f and

$$\mathbf{a}_r^{(f)} = [1, e^{-i2\pi f \mathbf{b}_r^T \mathbf{p}_2/c}, \ldots, e^{-i2\pi f \mathbf{b}_r^T \mathbf{p}_I/c}]^T \in \mathbb{C}^I \tag{35}$$

is now the frequency dependent steering vector associated with the rth signal at frequency f. As in the narrowband model (13), $\mathbf{p}_i$ denotes the position of the ith vector-sensor and $\mathbf{b}_r$ denotes the bearing vector associated with the rth source.

The set of tensors $\{\mathcal{Z}^{(f)}\}$ given by (34) clearly admits a coupled CPD interpretation. Hence, the uniqueness conditions and algorithms developed in [29], [32] for coupled CPD can directly be applied to the wideband VSA problem in (34). Note that we did not impose any particular geometry on the sensor array. Wideband VSA processing in the case of random array geometries is for instance relevant for sonobouys with arbitrary displacements due to the drifting in the water (e.g. [16]).

In VSA one of the involved factor matrices may be real. For instance, in acoustic VSA processing $\mathbf{d}_r$ in (34) takes the form $\mathbf{d}_r = [1,\ \sin(\phi_r)\cos(\theta_r),\ \sin(\phi_r)\sin(\theta_r),\ \cos(\phi_r)]^T$ [18]. We have already demonstrated in subsection III-C that this property can be exploited. In short, define $\mathcal{X}^{(f)} \in \mathbb{C}^{I\times M\times L}$ as follows $x^{(f)}_{iml} = z^{(f)*}_{iml}$. We now obtain the tensors $\{\mathcal{Z}^{(f)}, \mathcal{X}^{(f)}\}$ with coupled CPD of the form

$$\begin{cases} \mathcal{Z}^{(f)} = \sum_{r=1}^{R} \mathbf{a}_r^{(f)} \circ \mathbf{s}_r^{(f)} \circ \mathbf{d}_r\ , & f \in \{1,\dots,F\}, \\ \mathcal{X}^{(f)} = \sum_{r=1}^{R} \mathbf{a}_r^{(f)*} \circ \mathbf{s}_r^{(f)*} \circ \mathbf{d}_r\ , & f \in \{1,\dots,F\}. \end{cases}$$

In practice, the VSA is often regularly structured. For instance, in [1], [6], [20] the VSA is ULA structured. We stress that the result presented here is valid for any structured VSA enjoying a shift-invariance property. For simplicity, let us limit the discussion to the case of a ULA along the x-axis such that the array response vector (35) takes the form $\mathbf{a}_r^{(f)} = [1, x_r(f), \dots, x_r(f)^{I-1}]^T \in \mathbb{C}^I$, in which $x_r(f) = e^{-i2\pi f d_x \sin(\phi_r)\cos(\theta_r)/c}$ and d_x denotes the inter-element spacing along the x-axis. Using spatial smoothing we obtain the fourth-order tensors $\mathcal{V}^{(f)} \in \mathbb{C}^{K_{1,f}\times L_{1,f}\times M\times L}$ with factorizations

$$\mathcal{V}^{(f)} = \sum_{r=1}^{R} \mathbf{a}_r^{(K_1,f)} \circ \mathbf{a}_r^{(L_1,f)} \circ \mathbf{s}_r^{(f)} \circ \mathbf{d}_r\ , \quad f \in \{1,\dots,F\}, \quad (36)$$

where $\mathbf{a}_r^{(K_1,f)} = [1\ x_r(f)\ \dots\ x_r(f)^{(K_{1,f}-1)}]^T$ and $\mathbf{a}_r^{(L_1,f)} = [1\ x_r(f)\ \dots\ x_r(f)^{(L_{1,f}-1)}]^T$ are subject to $K_{1,f} + L_{1,f} = I + 1$. Clearly the factorization of the fourth-order tensors $\{\mathcal{V}^{(f)}\}$ in (36) admits a coupled CPD interpretation. The combination of coupled and higher-order structures leads to improved uniqueness conditions and algorithms, see [29], [32] for details.

VI. Numerical experiments

Consider the factorization $\mathbf{X} = \mathbf{A}\mathbf{S}^T$ in (13). The goal is to estimate the angles $\{\theta_r, \phi_r\}$ from $\mathbf{T} = \mathbf{X} + \beta\mathbf{N}$, where $\mathbf{N}$ is an unstructured perturbation matrix and $\beta \in \mathbb{R}$ controls the noise level. The angles $\{\theta_r, \phi_r\}$ are randomly chosen on the interval $[-\pi/2, \pi/2]$. The real and imaginary entries of the perturbation matrices are randomly drawn from a Gaussian distribution with zero mean and unit variance. The following Signal-to-Noise Ratio (SNR) measure will be used: SNR [dB] $= 10\log(\|\mathbf{X}\|_F^2/\|\beta\mathbf{N}\|_F^2)$. The performance evaluation will be based on the distance between the true angles $\{\theta_r, \phi_r\}$ and their estimates $\{\hat{\theta}_r, \hat{\phi}_r\}$. The distance is measured according to

$$\mathrm{E_{RMS}} = \min_{\sigma\in\Lambda_R} \sqrt{\frac{1}{R}\sum_{r=1}^{R} \left(\theta_r - \hat{\theta}_{\sigma(r)}\right)^2 + \left(\phi_r - \hat{\phi}_{\sigma(r)}\right)^2},$$

where Λ_R denotes the set of $R!$ possible permutations of the elements $\{1,\dots,R\}$ and $\sigma(r)$ denotes the rth element of the corresponding permuted set.

We compare the MHR-ESPRIT method [30], and briefly reviewed in the appendix, with the unitary 2D ESPRIT method developed for centro-symmetric arrays in [39]. In contrast to unitary 2D ESPRIT, MHR-ESPRIT method does not require that the individual subarrays yield unique DOAs.

A. Centro-symmetric cross-shaped array

Consider the CA in subsection IV-A2 with $I = J = 5$, $K = 50$ and $R = 4$. Furthermore, we set $\theta_2 = \theta_1$ and $\phi_4 = \phi_3$. Note that methods that only take one of the ULAs of the CA into account will not be able to recover the DOAs. We compare the unitary ESPRIT and ALS methods. The mean θ_{RMS} value over 200 trials as a function of SNR can be seen in figure 6. We note that the ALS method is very sensitive w.r.t. to its initialization. Below 25 dB the ALS-10 method yields a better estimate than the unitary ESPRIT method. The reason for this behaviour is that in the noise-free case unitary ESPRIT yields the exact solution, while at low SNR values the noise-free assumption is violated.

B. Asymmetric L-shaped array

Consider the LA in subsection IV-B with $I = J = 5$, $K = 50$ and $R = 5$. Note that methods that only take one of the ULAs of the CA into account will not be able to recover the DOAs. We compare the ESPRIT and ALS methods. The mean θ_{RMS} value over 200 trials as a function of SNR can be seen in figure 7. We observe the same behaviour as in the previous case.

VII. Conclusion

Despite its importance, sensor array processing still presents important algebraic challenges. We have first made a link between several narrowband sensor array processing problems and the coupled CPD. This has led to a new uniqueness condition for sensor array processing problems involving multiple shift-invariance structures. The coupled CPD also provides an algebraic MHR-ESPRIT method that under mild conditions is guaranteed to find the decomposition in the exact case.

Second, we made a link between wideband VSA processing and the coupled CPD. This has lead to an algebraic coherent data processing framework for wideband VSA, for which uniqueness conditions and algorithms can be developed based on the coupled CPD.

APPENDIX
MHR-ESPRIT FOR ARRAY PROCESSING

Let us briefly explain that the MHR-ESPRIT method [30] is also applicable for array processing. We limit the discussion to LAs and CAs used in Section VI. The derivation of MHR-ESPRIT variants for the other array configurations discussed in this paper is analogous.

Consider the LA depicted in figure 5. The output of the vertical and horizontal ULAs can be stacked into the matrices $\mathbf{X}^{(1)}$ and $\mathbf{X}^{(2)}$ according to $(\mathbf{X}^{(1)})_{ik} = x_{ik}$ and $(\mathbf{X}^{(2)})_{ik} = y_{ik}$. This leads to the matrix factorizations $\mathbf{X}^{(1)} = \mathbf{B}^{(1)}\mathbf{S}^T$ and $\mathbf{X}^{(2)} = \mathbf{B}^{(2)}\mathbf{S}^T$, where $\mathbf{b}_r^{(1)} = \begin{bmatrix}1 & x_{r,1} & x_{r,1}^2 & \dots & x_{r,1}^{I_1-1}\end{bmatrix}^T$ with $x_{r,1} = e^{-i\omega_c d_x \sin(\phi_r)\cos(\theta_r)/c}$ and $\mathbf{b}_r^{(2)} = \begin{bmatrix}1 & x_{r,2} & x_{r,2}^2 & \dots & x_{r,2}^{I_2-1}\end{bmatrix}^T$ with $x_{r,2} = e^{-i\omega_c d_y \sin(\phi_r)\sin(\theta_r)/c}$. Using spatial smoothing we obtain the tensors $\{\mathcal{Y}^{(1)}, \mathcal{Y}^{(2)}\}$ with coupled matrix representation $\begin{bmatrix}\mathbf{Y}^{(1)}\\ \mathbf{Y}^{(2)}\end{bmatrix} = \begin{bmatrix}\mathbf{A}^{(1)}\odot\mathbf{D}^{(1)}\\ \mathbf{A}^{(2)}\odot\mathbf{D}^{(2)}\end{bmatrix}\mathbf{S}^T$, where $\mathbf{A}^{(n)} = \underline{\mathbf{B}}^{(n)}$ and $\mathbf{D}^{(n)} = \mathbf{B}^{(n)}(1:2,:)$.

Assume that Theorem II.3 guarantees the uniqueness of the coupled CPD of $\{\mathcal{Y}^{(1)}, \mathcal{Y}^{(2)}\}$. Then $\begin{bmatrix}\mathbf{B}^{(1)}\\ \mathbf{B}^{(2)}\end{bmatrix}$ has full column rank. Indeed, if $\begin{bmatrix}\mathbf{B}^{(1)}\\ \mathbf{B}^{(2)}\end{bmatrix}$ does not have full column rank, then there exists a vector $\mathbf{y} \in \ker\left(\begin{bmatrix}\mathbf{B}^{(1)}\\ \mathbf{B}^{(2)}\end{bmatrix}\right)$ and a vector $\mathbf{x} \in \mathbb{C}^K$ such that $\begin{bmatrix}\mathbf{X}^{(1)}\\ \mathbf{X}^{(2)}\end{bmatrix} = \begin{bmatrix}\mathbf{B}^{(1)}\\ \mathbf{B}^{(2)}\end{bmatrix}(\mathbf{S} + \mathbf{x}\mathbf{y}^T)^T$ has rank $R-1$ which in turn will contradict Theorem II.3.

Let $\begin{bmatrix}\mathbf{X}^{(1)}\\ \mathbf{X}^{(2)}\end{bmatrix} = \mathbf{U}\Sigma\mathbf{V}^H$ denote the compact SVD of $\begin{bmatrix}\mathbf{X}^{(1)}\\ \mathbf{X}^{(2)}\end{bmatrix}$, where $\mathbf{U} \in \mathbb{C}^{I\times R}$ and $\mathbf{V} \in \mathbb{C}^{K\times R}$ are columnwise orthonormal and $\Sigma \in \mathbb{C}^{R\times R}$ is diagonal. We now know that $\text{range}\left(\begin{bmatrix}\mathbf{X}^{(1)}\\ \mathbf{X}^{(2)}\end{bmatrix}\right) = \text{range}(\mathbf{U})$ and that there exists a nonsingular matrix $\mathbf{F} \in \mathbb{C}^{R\times R}$ such that $\begin{bmatrix}\widetilde{\mathbf{U}}^{(1)}\\ \widetilde{\mathbf{U}}^{(2)}\end{bmatrix} := \mathbf{U}\Sigma = \begin{bmatrix}\mathbf{B}^{(1)}\\ \mathbf{B}^{(2)}\end{bmatrix}\mathbf{F}$, where $\widetilde{\mathbf{U}}^{(n)} \in \mathbb{C}^{I_n\times R}$. Spatial smoothing applied on $\widetilde{\mathbf{U}}^{(n)}$ yields $\mathcal{V}^{(n)} \in \mathbb{C}^{(I_n-1)\times 2\times R}$ with matrix representation $\mathbf{V}^{(n)} \in \mathbb{C}^{(I_n-1)2\times R}$, admitting the factorization $\mathbf{V}^{(n)} = \left(\mathbf{A}^{(n)} \odot \mathbf{D}^{(n)}\right)\mathbf{F}$. Overall, we obtain

$$\begin{bmatrix}\mathbf{V}^{(1)}\\ \mathbf{V}^{(2)}\end{bmatrix} = \begin{bmatrix}\mathbf{B}^{(1)} \odot \mathbf{D}^{(1)}\\ \mathbf{B}^{(2)} \odot \mathbf{D}^{(2)}\end{bmatrix}\mathbf{F}, \tag{37}$$

From (37) we build R symmetric matrices $\{\mathbf{M}^{(r)}\}$, admitting the factorizations

$$\mathbf{M}^{(r)} = \mathbf{G}\Lambda^{(r)}\mathbf{G}^T, \quad r \in \{1,\dots,R\}, \tag{38}$$

where $\mathbf{G} = \mathbf{F}^{-1}$ and $\Lambda^{(r)} \in \mathbb{C}^{R\times R}$ are diagonal matrices. See [27], [32] for the construction. After $\mathbf{G}$ has been found from (38) we compute $\mathbf{H} = \mathbf{U}\Sigma\mathbf{G}$ and partition it as follows $\mathbf{H} = \left[\mathbf{H}^{(1)T}, \mathbf{H}^{(2)T}\right]^T$, $\mathbf{H}^{(n)} \in \mathbb{C}^{2(I_n-1)\times R}$. The matrices $\mathbf{A}^{(n)}$ and $\mathbf{D}^{(n)}$ can now be obtained via the rank-1 approximations $\min_{\mathbf{a}_r^{(n)},\mathbf{d}_r^{(n)}} \left\|\mathbf{h}_r^{(n)} - \mathbf{a}_r^{(n)} \otimes \mathbf{d}_r^{(n)}\right\|_F^2$, where $r \in \{1,\dots,R\}$ and $n \in \{1,2\}$. The goal is now to recover the generators $\{x_{r,n}\}$ from $\mathbf{A}^{(n)}$ and $\mathbf{D}^{(n)}$. Define

$$\mathbf{c}_r^{(1,n)} = \begin{bmatrix}\underline{\mathbf{a}}_r^{(n)} \otimes \mathbf{d}_r^{(n)}\\ \mathbf{a}_r^{(n)} \otimes \underline{\mathbf{d}}_r^{(n)}\end{bmatrix}, \quad \mathbf{c}_r^{(2,n)} = \begin{bmatrix}\overline{\mathbf{a}}_r^{(n)} \otimes \mathbf{d}_r^{(n)}\\ \mathbf{a}_r^{(n)} \otimes \overline{\mathbf{d}}_r^{(n)}\end{bmatrix}.$$

Then the generator $x_{r,n}$ follows from the relation $\mathbf{c}_r^{(n)}x_r^n = \mathbf{d}_r^{(n)}$. Using the identities $\cos(\phi_{r,n}) = \cos^2(\phi_{r,n}/2) - \sin^2(\phi_{r,n}/2)$ and $\sin(\phi_{r,n}) = 2\sin(\phi_{r,n}/2)\cos(\phi_{r,n}/2)$ the LS estimate of $x_{r,n} = e^{i\cdot\phi_{r,n}}$ can be determined from

$$\begin{aligned} f(\phi_{r,n}) &= \left\|\mathbf{c}_r^{(1,n)}x_{r,n} - \mathbf{c}_r^{(2,n)}\right\|_F^2 \\ &= \alpha_n - 2\text{Re}\{\beta_n\}\cos(\phi_r) - 2\text{Im}\{\beta_n\}\sin(\phi_{r,n}) \\ &= \alpha_n - 2\text{Re}\{\beta_n\}\left(\cos^2(\phi_{r,n}/2) - \sin^2(\phi_{r,n}/2)\right) \\ &- 4\text{Im}\{\beta_n\}\sin(\phi_{r,n}/2)\cos(\phi_{r,n}/2) \\ &= \alpha_n - \begin{bmatrix}\cos(\phi_{r,n}/2)\\ \sin(\phi_{r,n}/2)\end{bmatrix}^T \mathbf{G}^{(n)} \begin{bmatrix}\cos(\phi_{r,n}/2)\\ \sin(\phi_{r,n}/2)\end{bmatrix}, \end{aligned}$$

where $\alpha_n = \mathbf{c}_r^{(1,n)H}\mathbf{c}_r^{(1,n)} + \mathbf{c}_r^{(2,n)H}\mathbf{c}_r^{(2,n)}$, $\beta_n = \mathbf{c}_r^{(1,n)H}\mathbf{c}_r^{(2,n)}$ and $\mathbf{G}^{(n)} = 2\begin{bmatrix}-\text{Re}\{\beta_n\} & \text{Im}\{\beta_n\}\\ \text{Im}\{\beta_n\} & \text{Re}\{\beta_n\}\end{bmatrix}$. Let $\mathbf{x}^{(n)} \in \mathbb{R}^2$ denote the eigenvector associated with the dominant eigenvalue of $\mathbf{G}^{(n)}$, then we obtain $\phi_{r,n} = 2\tan^{-1}\left(x_2^{(n)}/x_1^{(n)}\right)$. Compute $y_{r,1} = -\phi_{r,1}(\omega_c d_x)/c = \sin(\phi_r)\cos(\theta_r)$, $y_{r,2} = -\phi_{r,2}(\omega_c d_y)/c = \sin(\phi_r)\sin(\theta_r)$ and $w_r = y_{r,1} + iy_{r,2} = \sin(\phi_r)(\cos(\theta_r) + i\sin(\theta_r)) = \sin(\phi_r)e^{i\theta_r}$. Then $\theta_r = \angle w_r$ and $\phi_r = \sin^{-1}(|w_r|)$.

REFERENCES

[1] H.-W. Chen and J.-W. Zhao, "Wideband MVDR beamforming for acoustic sensor linear array," *IEE Proc.-Radar, Sonar Navig.*, vol. 151, no. 3, pp. 158–162, Jun. 2004.

[2] L. De Lathauwer, "A link between the canonical decomposition in multilinear algebra and simultaneous matrix diagonalization," *SIAM J. Matrix Anal. Appl.*, vol. 28, no. 3, pp. 642–666, 2006.

[3] I. Domanov and L. De Lathauwer, "On the uniqueness of the canonical polyadic decomposition of third-order tensors — Part I: Basic results and uniqueness of one factor matrix," *SIAM J. Matrix Anal. Appl.*, vol. 34, no. 3, pp. 855–875, 2013.

[4] ——, "On the uniqueness of the canonical polyadic decomposition of third-order tensors — Part II: Overall uniqueness," *SIAM J. Matrix Anal. Appl.*, vol. 34, no. 3, pp. 876–903, 2013.

[5] ——, "Canonical polyadic decomposition of third-order tensors: reduction to generalized eigenvalue decomposition," *SIAM J. Matrix Anal. Appl.*, vol. 35, no. 2, pp. 636–660, 2014.

[6] D. Donno, A. Nehorai, and U. Spagnolini, "Seismic velocity and polarization estimation for wavefield separation," *IEEE Trans. Signal Process.*, vol. 56, no. 10, Oct. 2008.

[7] R. Eckhoff, "Direction-of-arrival determination using 3-axis crossed array and ESPRIT," in *Proc. of the 9th IEEE International Symposium PIMRC 1998*, september 8-11, Boston, MA, USA, 1998.

[8] T. Filik and E. Tuncer, "Uniform and nonuniform V-shaped isotropic planar arrays," in *Proc. of the 5th IEEE SAM Workshop*, july 21-23, Darmstadt, Germany, 2008.

[9] H. Gazzah and S. Marcos, "Cramer-Rao bounds for antenna array design," *IEEE Trans. Signal Process.*, vol. 54, no. 1, pp. 336–345, Jan. 2006.

[10] X. Guo, S. Miron, D. Brie, S. Zhu, and X. Liao, "A CANDECOMP/PARAFAC perspective on uniqueness of DOA estimation using a vector sensor array," *IEEE Trans. Signal Process.*, vol. 59, no. 7, pp. 3475–3481, Jul. 2011.

[11] Y. Hua and T. K. Sarkar, "A note on the Cramer-Rao bound for 2-D direction finding based on 2-D array," *IEEE Trans. Signal Process.*, vol. 39, no. 5, pp. 1215–1218, May 1991.

[12] Y. Hua, T. K. Sarkar, and D. D. Weiner, "An L-shaped array for estimating 2-D directions of wave arrival," *IEEE Trans. Antennas. Propag.*, vol. 39, no. 2, pp. 143–146, Feb. 1991.

[13] T. Jiang and N. D. Sidiropoulos, "Kruskal's permutation lemma and the identification of CANDECOMP/PARAFAC and bilinear model with constant modulus constraints," *IEEE Trans. Signal Process.*, vol. 52, no. 9, pp. 2625–2636, Sep. 2004.

[14] T. Koruda, N. Kikuma, and N. Inagaki, "DOA estimation and pairing method in 2D-ESPRIT using triangular antenna array," *Electronics and Communications in Japan*, vol. 86, no. 6, pp. 1505–1513, 2003.

[15] L.-H. Lim and P. Comon, "Blind multilinear identification," *IEEE Trans. Inf. Theory*, vol. 60, no. 2, pp. 1260–1280, Feb. 2014.
[16] A. Massoud, A. Osman, and A. Noureldin, "DOA estimation based on fourth order cumulant beamforming for nonunifom linear array of DIFAR sonobuoys," *Comput. Electr. Eng.*, vol. 38, no. 4, pp. 986–993, Jul. 2012.
[17] S. Miron, Y. Song, D. Brie, and T. Wong, "Candecomp/Parafac (CP) direction finding with multi-scale array," in *Proc. of the 5th IEEE Workshop CAMSAP*, December 15-18, Saint Martin, Dutch Antilles, 2013.
[18] A. Nehorai and E. Paldi, "Acoustic vector-sensor array processing," *IEEE Trans. Signal Process.*, vol. 42, no. 9, pp. 2481–2491, Sep. 1994.
[19] ——, "Vector-sensor array processing for electromagnetic source localization," *IEEE Trans. Signal Process.*, vol. 42, no. 2, pp. 376–398, Feb. 1994.
[20] C. Paulus and J. I. Mars, "Vector-sensor array processing for polarization parameters and DOA estimation," *EURASIP Journal on Advances in Signal Processing*, 2010, article ID 850265.
[21] S. U. Pillai and B. H. Kwon, "Forward/backward spatial smoothing techniques for coherent signal identification," *IEEE Trans. Acoust., Speech, Signal Processing*, vol. 37, no. 1, pp. 8–15, Jan. 1989.
[22] R. Roy and T. Kailath, "Estimation of signal parameters via rotational invariance techniques," *IEEE Trans. Acoust., Speech, Signal Processing*, vol. 32, no. 7, pp. 984–995, Jul. 1989.
[23] T. J. Shan, M. Wax, and T. Kailath, "On spatial smoothing for direction-on-arrival of coherent signals," *IEEE Trans. Acoust., Speech, Signal Processing*, vol. 33, no. 8, pp. 806–811, Aug. 1985.
[24] N. D. Sidiropoulos, R. Bro, and G. B. Giannakis, "Parallel factor analysis in sensor array processing," *IEEE Trans. Signal Processing*, vol. 48, no. 8, pp. 2377–2388, Aug. 2000.
[25] L. Sorber, M. Van Barel, and L. De Lathauwer, "Structured data fusion," ESAT-STADIUS, KU Leuven, Belgium, Tech. Rep. 13-177, 2013.
[26] M. Sørensen and L. De Lathauwer, "Coupled tensor decompositions for applications in array signal processing," in *Proc. CAMSAP 2013*, Dec. 15-18, Saint Martin, Dutch Antilles, 2013.
[27] ——, "Multidimensional ESPRIT: A coupled canonical polyadic decomposition approach," in *Proc. of the 8th IEEE SAM Workshop*, Jun. 22-25, A Coruna, Spain, 2014.
[28] ——, "Blind signal separation via tensor decompositions with a Vandermonde factor: Canonical polyadic decomposition," *IEEE Trans. Signal Processing*, vol. 61, no. 22, pp. 5507–5519, Nov. 2013.
[29] ——, "Coupled canonical polyadic decompositions and (coupled) decompositions in multilinear rank-($L_{r,n}$, $L_{r,n}$, 1) terms — Part I: Uniqueness," ESAT-STADIUS, KU Leuven, Belgium, Tech. Rep. 13-143, 2013.
[30] ——, "Multidimensional harmonic retrieval via coupled canonical polyadic decompositions," ESAT-STADIUS, KU Leuven, Belgium, Tech. Rep. 13-240, 2013.
[31] ——, "New uniqueness conditions for the canonical polyadic decomposition of third-order tensors," ESAT-STADIUS, KU Leuven, Belgium, Tech. Rep. 13-05, 2013.
[32] M. Sørensen, I. Domanov, D. Nion, and L. De Lathauwer, "Coupled canonical polyadic decompositions and (coupled) decompositions in multilinear rank-($L_{r,n}$, $L_{r,n}$, 1) terms — Part II: Algorithms," ESAT-STADIUS, KU Leuven, Belgium, Tech. Rep. 13-144, 2013.
[33] P. Stoica and R. L. Moses, *Spectral analysis of signals*. Prentice Hall, 2005.
[34] A. Swindlehurst and T. Kailath, "Azimuth/elevation direction finding using regular array geometries," *IEEE Trans. Aerosp. Electron. Syst.*, vol. 29, no. 1, pp. 145–156, Jan. 1993.
[35] A. Swindlehurst, B. Ottersten, R. Roy, and T. Kailath, "Multiple invariance ESPRIT," *IEEE Trans. Signal Process.*, vol. 40, no. 4, pp. 868–881, Apr. 1992.
[36] A. Swindlehurst, P. Stoica, and M. Jansson, "Exploiting arrays with multiple invariances using MUSIC and MODE," *IEEE Trans. Signal Process.*, vol. 49, no. 11, pp. 2511–2521, Nov. 2001.
[37] Z. Tian and H. L. Van Trees, "DOA estimation with hexagonal arrays," in *Proc. ICASSP*, May 12-15, Seattle, WA, USA, 1998.
[38] S. Zhao, T. Saluev, and D. L. Jones, "Underdetermined direction of arrival estimation using acoustic vector sensor," *Signal Processing*, vol. 100, no. 1, pp. 160–168, 2014.
[39] M. D. Zoltowski, M. Haardt, and C. P. Matthews, "Closed-form 2-D angle estimation with rectangular arrays in element space or beamspace via unitary ESPRIT," *IEEE Trans. Signal Process.*, vol. 44, no. 2, pp. 316–328, Feb. 1996.

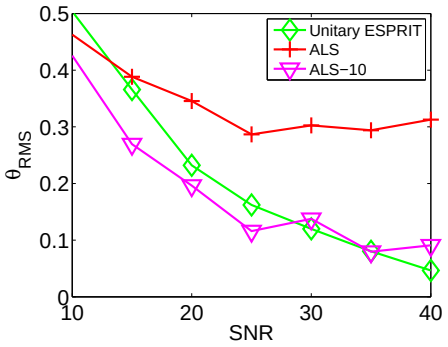

Fig. 6. Mean θ_{RMS} values over 200 trials while SNR is varying from 10 to 40 dB, cross-shaped array.

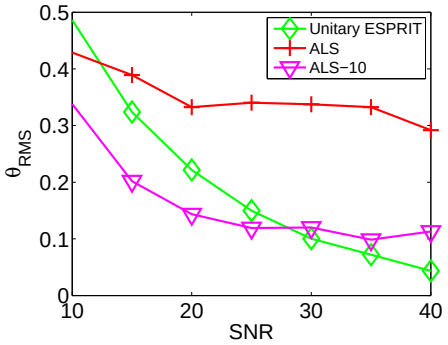

Fig. 7. Mean θ_{RMS} values over 200 trials while SNR is varying from 10 to 40 dB, L-shaped array.

Acknowledgment

Research supported by: (1) Research Council KU Leuven: CoE EF/05/006 Optimization in Engineering (OPTEC), (2) F.W.O.: project G.0427.10N, G.0830.14N, G.0881.14N, (3) the Belgian Federal Science Policy Office: IUAP P7 (DYSCO II, Dynamical systems, control and optimization, 2012–2017), (4) EU: The research leading to these results has received funding from the European Research Council under the European Union's Seventh Framework Programme (FP7/2007-2013) / ERC Advanced Grant: BIOTENSORS (no. 339804). This paper reflects only the authors' views and the Union is not liable for any use that may be made of the contained information.

Mikael Sørensen received the Master's degree from Aalborg University, Denmark, and the Ph.D. degree from University of Nice, France, in 2006 and 2010, respectively, both in electrical engineering. Since 2010 he has been a Postdoctoral Fellow with the KU Leuven, Belgium. His research interests include applied linear algebra, tensor decompositions, and tensor-based signal processing.

Lieven De Lathauwer received the Master's degree in electromechanical engineering and the Ph.D. degree in applied sciences from KU Leuven, Belgium, in 1992 and 1997, respectively. He is currently Professor with KU Leuven, Belgium. Dr. De Lathauwer is an Associate Editor of the SIAM Journal on Matrix Analysis and Applications and has served as an Associate Editor for the IEEE Transactions on Signal Processing. His research concerns the development of tensor tools for engineering applications.